Microporous and Mesoporous Materials 315 (2021) 110919

Contents lists available at ScienceDirect

Microporous and Mesoporous Materials

journal homepage: http://www.elsevier.com/locate/micromeso

# Facile strategies for synthesis of functionalized mesoporous silicas for the removal of rare-earth elements and heavy metals from aqueous systems

O. Dudarko [a,*], N. Kobylinska [b], B. Mishra [c], V.G. Kessler [d], Bijay P. Tripathi [c,**], G. A. Seisenbaeva [d,***]

[a] Chuiko Institute of Surface Chemistry of NAS of Ukraine, 17 General Naumov Str., Kyiv, 03164, Ukraine
[b] Department of Analytical Chemistry, Taras Shevchenko National University of Kyiv, 64/13, Volodymyrska Str., Kyiv, 01601, Ukraine
[c] Department of Materials Science & Engineering, Indian Institute of Technology Delhi, Hauz Khas, New Delhi, 110016, India
[d] Department of Molecular Sciences, Swedish University of Agricultural Sciences, 75007, Uppsala, Sweden

ARTICLE INFO

*Keywords:*
Ordered mesoporous silica
Adsorption
Heavy metal ions
Recovery
Water purification

ABSTRACT

A series of adsorbents of SBA-15-type with ethylenediaminetriacetic (EDTA), phosphonic, and ammonium groups as ligands were synthesized using the template method based on sodium metasilicate as the major starting reagent. The detailed characterizations using SEM, TEM, XRD, and $N_2$ sorption/desorption measurements of synthesized sorbents confirmed an ordered mesoporous structures with uniform pore diameter and large surface area. Regardless of the functional groups concentration, the synthesized sorbents showed significantly higher adsorption capacities for target ions than neat SBA-15. The observed adsorption mechanisms were predominantly based on complexation and electrostatic interactions between metal ions and various functional groups present on the adsorbent surfaces. The synthesized SBA-15 derivatives were used for removal of different metal ions such as Fe(III), Ni(II), Cu(II), Pb(II), Nd(III), and Dy(III) from water (pH $\geq$ 1). The highest adsorption capacity was obtained for the bifunctional (-EDTA/phosphonic groups) modified adsorbent, reaching up to 119.05 mg $g^{-1}$ for Fe(III), 246.95 mg $g^{-1}$ for Pb(II), 246.95 mg $g^{-1}$ for Cu(II), 238.10 mg $g^{-1}$ for Nd(III) and 243.90 mg $g^{-1}$ for Dy(III). The adsorption data were successfully fitted to the Langmuir and Freundlich models, revealing a monolayer chemisorption of REEs on the mesoporous samples. Metal desorption and adsorbent recycling were also found to be efficient under acidic condition (0.5–1.0 M). These properties highlight the perspective uses of functionalized mesoporous silicas for the rapid and potentially selective removal of REEs and heavy metal ions from the complex water samples and technological mixtures.

## 1. Introduction

Water purification is one of the grand challenges faced worldwide during the 21st century to provide clean drinking water [1]. Clean water and sanitation have been identified as one of the United Nations Sustainable development goals. Growth of industries such as metal plating, mining, resistors, capacitors, laser, batteries, paper, and magnets led to rise in the effluent quantity containing metals, which are directly or indirectly discharged into the aquatic environments, especially in developing countries. These toxic heavy metals and rare earth elements (REEs) present in the wastewater should be removed and separated for their reuse. REEs possess chemical properties very similar to each other and with other neighboring elements of the periodic table, making their separation an arduous task. Methods such as chemical precipitation, ion-exchange, membrane filtration, and electrochemical treatment technologies are currently used to remove heavy metal ions from wastewaters [2]. However, solid adsorbents are considered to be a more appropriate method exploiting chemical bonding to and physical interactions with solid surfaces. Adsorption is now broadly recognized as an effective and economical method for pre-concentration and separation of metal ions [3]. Pore size, pore size distribution, and specific surface area and pore surface chemistry are significant factors in the adsorption process [4]. In particular, activated carbons have been extensively employed to purify contaminated waters due to their high

* Corresponding author.
** Corresponding author.
*** Corresponding author.
*E-mail address:* odudarko80@gmail.com (O. Dudarko).

https://doi.org/10.1016/j.micromeso.2021.110919
Received 15 July 2020; Received in revised form 19 January 2021; Accepted 20 January 2021
Available online 29 January 2021
1387-1811/© 2021 Elsevier Inc. All rights reserved.

surface area, stability, and durability under harsh conditions [5]. However, their random pore geometry and microporosity restrict the access of active sites for pollutant adsorption, and therefore, the selectivity, removal efficiency, and the adsorption kinetics are compromised.

Hybrid mesoporous materials, modified with functional groups, are often considered as better adsorbents than conventional activated carbon based materials for a range of pollutants, including toxic substances [6,7]. Ordered mesoporous silicas possess a large surface area with good physicochemical stability permitting to further functionalize them using various surface chemistry approaches. The periodic surface structure of mesoporous silica is of great advantage. It ensures the structural orientation of guest molecules in the pores, resulting in increased selectivity and sufficient adsorption capacity of the sorbents [6]. The SBA-15 mesostructured silica [8] consists of ordered hexagonal cylindrical pores that provide high surface area, and it is widely used in catalysis, sensor, and separation applications [9,10]. While mesoporous silica is usually more expensive than many other adsorbents, it offers several advantages making it more attractive. SBA-15 offers narrow pore size distribution and a wide range of controllable pore sizes (ranges from 5 to 30 nm), which permits target molecules to reach the inside surface of materials that fasten the physiochemical kinetics process [11]. However, to resolve this issue, SBA-15 is most often modified with several functional groups to tailor the surface properties and adsorption capacity.

Modifications of SBA-15 surface with organic species for adsorption applications have been extensively reported [12]. Functional groups, such as thiol [13, 14], amino [15], phosphorus-containing groups [16], iminodiacetic [17], and ethylenediaminetriacetic acid (EDTA) [18], were incorporated into the SBA-15 network for adsorption applications using co-condensation (one pot-synthesis) and grafting (post-synthesis) routes [12]. The thiol-functionalized SBA-15 silica showed exceptional selectivity for $Hg^{2+}$ [13] and noble metals adsorption from wastewater [14]. Amino-functionalized SBA-15 showed higher affinity for different metal ions, such as $Cu^{2+}$, $Zn^{2+}$, $Cr^{3+}$ and $Ni^{2+}$ [14], whereas the iminodiacetic acid-modified SBA-15 hybrid material showed high $Cd^{2+}$ adsorption from aqueous solutions [17]. At the same time, it was reported that EDTA-functionalized SBA-15 binds efficiently with $Cu^{2+}$ ions, in comparison with Cu(II) and other late transition ions on bare silica [19]. Synthesis of materials with carboxylic acid residues may involve additional functional groups to improve product performance for specific requirements. However, not all functional carboxylic groups are available for interaction [19]. P-containing groups are strong complexing ligands for transition metal ions and have high affinity for REEs [19,20]. P-containing ligands' coordination properties are used, for example, in the processes of extraction and separation of REEs [21]. In our previous studies, we also observed the interaction of multiply charged ions, including $Nd^{3+}$ and $Dy^{3+}$, with SBA-15 matrix modified by phosphonic acid derivatives resulting in maximal adsorption capacity of ~85 mg $g^{-1}$ for $Nd^{3+}$ [22].

Simultaneous introduction of functional groups of different nature in the surface layer often leads to manifestation of the cooperative effect for water treatment [23,24]. Introducing an amino acid and a carboxylic acid group imparts acid-base properties on the surface, possibly due to the analogy with an amino acid effect in many biological processes [25]. Materials with carboxylic acid/secondary amine, carboxylic acid/-pyridine, and carboxylic acid/phosphine pairs have been synthesized and investigated [26]. Apart from other advantages, the most attractive feature of amphoteric amino acid fragments is their ability to instantly switch from one state to another by specific parameters like pH. The cationic and acidic fragments are changed to anionic and basic by increasing pH of the solution [26,27]. The main advantage of these acid-base co-operative materials is their ability to regenerate the activity due to the rapid proton transfer between the basic and acidic groups [28]. Combining the phosphorus- and amino-containing moieties in one organo-inorganic material can potentially provide better extraction ability and allow for selectively target metal ions via formation of the more stable chelate complexes.

Selective sorption and separation of complex natural mixtures of ions have been less explored until now. Recently the separation of REEs with mixture of various ions including heavy metals have started getting attention. The interest to REEs, and especially neodymium (III) and dysprosium (III), are explained by focusing on recycling REE-containing End-of-Life products, for example, NdFeB magnets [29]. A drastic improvement in End-of-Life recycling rates for REEs is a strategic necessity. Recycling can help to reduce fluctuations of prices by reducing the potential for monopolies, even if recycling cannot totally replace the supply of REEs from mines. Practical application of new adsorbents for the extraction of REEs from such technological mixtures is still not matured.

This study is aimed at investigating the feasibility of using EDTA, phosphonic (-$PO(OH)_2$), and ammonium (-$NH_3^+Cl^-$) groups functionalized SBA-15-based mesoporous materials as adsorbents for the removal of REEs from the mixtures of metal ions in an aqueous solution. Herein, we are proposing simple techniques for the synthesis of relatively cheaper mono- and bi-functionalized organosilica adsorbents. Among many quests to be answered in this paper, our main focus is the procedure for separation of the REEs from the aqueous mixture containing other heavy metals monitored by UV–vis spectroscopy and inductively coupled plasma-optical emission spectrometry (ICP-OES) measurements using synthesized SBA-15-based adsorbents. Also, the nature and accessibility of adsorbing species in surface reactive sites located on the pore walls were studied. The effect of functional groups' availability inside the SBA-15 pores on adsorption mechanism for metal ions was also analyzed. Further, the nature of functional groups and their mechanisms in the uptake of metal ions from a complex mixture was also investigated. The impact to Nd(III) and Dy(III) ions is explained by focusing on the potential use of the obtained adsorbents for recycling of the End-of-Life products. Finally, metal ions desorption and recycling of obtained adsorbents were investigated.

## 2. Experimental

### 2.1. Materials

Sodium metasilicate ($Na_2SiO_3{\cdot}9H_2O$, SS), aminopropyltriethoxysilane ($(C_2H_5O)_3Si(CH_2)_3NH_2$, APTES, 98%), 3-aminopropylsilanetriol $(HO)_3Si(CH_2)_3NH_2$, Gelest, 22–25% in water), trisodium salt of *N*-(triethoxysilylpropyl) ethylenediaminetriacetic acid ($(C_2H_5O)_3Si(CH_2)_3N(CH_2CO_2Na)CH_2CH_2N(CH_2CO_2Na)_2$ (EDTA), 40% in water) were obtained from Sigma-Aldrich USA. Diethylphosphatoethyltriethoxysilane ($(C_2H_5O)_3Si\ (CH_2)_2P(O)\ (OC_2H_5)_2$ (DPTES), 92%) was obtained from Gelest. Pluronic 123, ethanol, conc. Hydrochloric acid, heavy metal salts, fixanal solutions of magnesium sulfate ($MgSO_4$), ethylenediamine tetraacetic acid, sodium nitrate, sodium hydroxide, ammonium hydroxide, xylenol orange, 10% solution KSCN, Arsenazo III were obtained from Sigma-Aldrich USA unless otherwise stated. For all purposes, MilliQ water (Milli-Q® Integral system A10® Total Oxidizable Carbon) was used.

Model solution: 0.0277 mol $L^{-1}$ $Nd(NO_3)_3{\cdot}6H_2O$ (99.9%, Sigma-Aldrich), 0.0594 mol $L^{-1}$ $Fe(NO_3)_3{\cdot}9H_2O$ (≥98%,Sigma-Aldrich), 0,00276 mol $L^{-1}$ $Dy(NO_3)_3{\cdot}6H_2O$ (99.9%, Sigma-Aldrich), 0.004 mol $L^{-1}$ $Ni(NO_3)_2{\cdot}6H_2O$, 0.0057 mol $L^{-1}$ $H_3BO_3$ (99.5%, Sigma-Aldrich), 0.000273 mol $L^{-1}$ $Al(NO_3)_3{\cdot}9H_2O$ (97%, Sigma-Aldrich). Iron standard solution, 1000 mg $L^{-1}$ Fe in 0.5 M nitric acid (from $Fe(NO_3)_3$) Certipur® standard for AAS, Supelco®, Merck.

### 2.2. Synthesis of mesoporous silica type SBA-15 (SBA)

4 g of surfactant (Pluronic 123) was dissolved in the mixture of 60 mL of water and 36.8 mL of concentrated HCl under constant stirring during 30 min in a water bath at 40 °C. Then, 8.48 g of SS separately dissolved in 20 mL of water was added without interrupting the stirring. The sedimentation started immediately and completed in about 10 min.

The obtained mixture was further stirred for 2 h under the same conditions. After that, the hydrothermal treatment (HTT) was carried out at 80 °C for 20 h followed by the filtration of white precipitate. The above obtained material was air-dried overnight and the template was removed by boiling in an acidified ethanol for four times under stirring for 3 h. The filtered material was vacuum dried for half an hour at RT, followed by another half an hour at 50 °C, and a further 3 h at 100 °C.

### 2.3. Synthesis of SBA-NH (10:1)

The procedure described in section 2.2 was followed for SBA-NH synthesis also by adding 0.0016 mol of APTES to the template solution under stirring for 30 min, followed by the addition of 0.016 mol SS solution.

### 2.4. Synthesis of SBA-EDTA-NH (10:1:1)

The surfactant was dissolved in water at constant stirring at room temperature. Then concentrated hydrochloric acid was added to the clear solution. Without interrupting the stirring, 0.002 mol EDTA and 0.002 mol APTS were added at room temperature. SS (0.02 mol) was separately dissolved in water and added to the transparent template solution under continuous stirring at room temperature. After precipitation, the sample was stirred for 2 h at 40 °C and HTT was carried out for 20 h at 80 °C. After drying, the sample was boiled in ethanol (30 $cm^3$ per 1 g) 4 times for 3 h. After that the obtained sample was dried for 0.5 h without heating, followed by 0.5 h at 50 °C, and 3 h at 100 °C.

### 2.5. Synthesis of SBA-EDTA-NH1 (5:1:1)

For the synthesis of SBA-EDTA-NH1 same procedure as described in section 2.4 was followed with half of the amount of SS.

### 2.6. Synthesis of SBA-EDTA (20:1)

The synthesis of mesoporous materials with parameters close to SBA-15 with EDTA is possible only at a SS/EDTA ratio of 20:1. Procedure similar to the synthesis of SBA-EDTA-NH was used with only EDTA. No APTS or APTES were used in this synthesis.

### 2.7. Synthesis of SBA-EDTA-POOH1. (10:1:1)

As described in previous sections, 0.0035 mol EDTA with hydrolyzed 0.0035 mol DPTS and a 0.035 mol SS was used in this synthesis. DPTS was pre-hydrolyzed in a strongly acidic medium to transform phosphate functional groups into $\equiv Si(CH_2)_2P(O)(OH)_2$. Under these conditions, ethoxy-groups both at phosphorus and silicon atoms were hydrolyzed to form a colorless and highly water-soluble oligomers [30].

### 2.8. Synthesis of SBA-EDTA-POOH (20:1:1)

Procedure adopted in section 2.7 was used for the synthesis of SBA-EDTA-POOH except the SS was taken as 0.07 mol.

Details of the reaction ratios of various components for the synthesis of all adsorbents are summarized in Table 1.

### 2.9. Instrumental characterizations

For morphology examination and elemental composition determination, a Hitachi TM-3000 scanning electron microscope (SEM) was used. Transmission electron microscope (TEM) micrographs of samples were obtained using a SELMI PES-125K microscope at an accelerating voltage of 100 kV. The adsorbents were crushed and ultrasonicated to disperse in ethyl alcohol at room temperature.

TGA experiment was performed using a TA-Q500 thermal analyzer (TA Instruments, USA) in the temperature range of 20–800 °C at a heating rate of 10 °C/min under nitrogen atmosphere. TGA and DTG (Derivative thermogravimetric) curves were obtained using TA Universal analysis software.

Infrared spectra of all samples were recorded using tablets with KBr (1:20). The FTIR spectrophotometer (Nicolet NEXUS 470) with the SMART Collector diffusion reflector was used to record IR spectra in the range 400–4000 $cm^{-1}$. In all cases, 50 scans with a resolution of 8 $cm^{-1}$ were used.

Powder XRD data for samples were measured using the DRON-4-07 diffractometer (Open Joint-Stock Company Scientific and Production Enterprise "Burevestnik", Russ. Fed.), equipped with $CuK_\alpha$ radiation (40 kV, 20 mA) at the rate of 0.1°/min over the low-angle range (0.5–3°).

Electrophoretic mobility measurements were carried out with Zeta-Sizer Nano ZS Analyzer (Malvern Instruments, UK) at room temperature and external electric field gradients of 6–15 V/cm. All measurements were performed in dilute suspensions of various adsorbents in aqueous solutions, at different ionic strength values and in broad pH range. Solutions of NaOH and HCl were employed to adjust the pH values of the suspensions. The electrophoretic mobility values were converted into electrokinetic potentials by the classical Smoluchowski formula using the software package supplied with the instrument. The resulting ζ-potentials were obtained by averaging the data of three to five individual measurements. The error of the measurements was estimated to be in the range of 2–3%.

Textural properties of the mesoporous matrices were determined from the $N_2$ adsorption isotherms recorded at 77 K with a Kelvin-1042 apparatus (Costech Instruments). The samples were initially degassed in a helium flow at 110 °C for 1 h under a vacuum ($10^{-4}$ mbar) to ensure a clean, dry surface, free of any loosely bound adsorbed species. The volume of adsorbed gas was determined at the time of establishing quasi-equilibrium in the gas flow, which was monitored by a thermal conductivity detector (measurement accuracy was ±3%). The specific surface area ($S_{BET}$) of samples was determined by BET method [31]. The pore diameter and pore size distributions were calculated from the desorption branches of the corresponding nitrogen isotherm using the BJH [32] and modified Nguyen-Do method (MND method) [33,34].

Nitrogen, Carbon, and Hydrogen contents in the silica samples were determined by using a Vario MACRO cube elemental analyzer (Germany) connected with a thermal conductivity detector. Sulphanilamide was used as a standard.

The concentration of available functional groups on the silica surface was determined by potentiometric titration (I-160M). A batch of the sample (0.0500 ± 0.0005 g) was poured into 25 mL of 0.1 M $NaNO_3$, incubated for 24 h, and titrated with 0.1 M NaOH solution.

**Table 1**
The ratio of alkoxysilanes and other reagents in the reaction mixture.

| Sample | Functional groups | SS (mmol) | EDTA (mmol) | APTES (mmol) | APTS (mmol) | DPTS (mmol) |
|---|---|---|---|---|---|---|
| SBA | -OH | 10 | - | - | - | - |
| SBA-EDTA | -OH/-EDTA | 20 | 1 | - | - | - |
| SBA-NH | -OH/-$NH_3^+Cl^-$ | 10 | - | 1 | - | - |
| SBA-EDTA-NH1 | -OH/-$NH_3^+Cl^-$/-EDTA | 5 | 1 | - | 1 | - |
| SBA-EDTA-NH | -OH/-$NH_3^+Cl^-$/-EDTA | 10 | 1 | - | 1 | - |
| SBA-EDTA-POOH1 | -OH/-$PO(OH)_2$/-EDTA | 10 | 1 | - | - | 1 |
| SBA-EDTA-POOH | -OH/-$PO(OH)_2$/-EDTA | 20 | 1 | - | - | 1 |

### 2.10. Adsorption experiments

#### 2.10.1. Determination of metal contents

Metal concentrations (ppm level) in both initial and final solutions were determined by spectrophotometry using Shimadzu UV-1800 spectrometer.

*Determination of Fe(III).* Fe(III) content was determined by spectrophotometric method based on reaction with thiocyanate in the nitric acid medium using 470 nm wavelength. Briefly, the solution containing 10–30 mg of Fe(III) (1 mL of studied supernatant) with pH~1 was added to 5 mL of KSCN (10%) solution in a volumetric flask and brought to 50 mL with water. The calibration curve was constructed from a working solution after diluting standard solution: $A_{470} = 84.7 \cdot C_{Fe}$-0.0129, $R^2 = 0.9824$. Studies were conducted using the blank solution as a reference.

*Determination of Nd(III).* In a typical experiment, the concentration of Nd(III) in the supernatant was determined using Arsenazo III by spectrophotometry at wavelength 672 nm (the detection limit of the procedure was below 0.1 ppm). Before the determination, the solution was diluted 2.5–10 times to achieve the Nd(III) concentration in the range 0–16 μg $mL^{-1}$. The calibration plot was constructed from a working solution of $Nd(NO_3)_3$ after diluting standard solution: $A_{672} = 0.0033 \cdot C_{Nd}+0.0082$, $R^2 = 0.9966$.

The liquid phase (solution after metal adsorption and the eluate) was analyzed for metal content at trace level for REEs and heavy metals by ICP-OES (iCAP 6300 Thermo Scientific, USA), respectively. The metal ions emission lines used were at 315.887 nm (Ca), 267.716 nm (Cr), 259.940 nm (Fe), 224.700 nm (Cu), 220.353 nm (Pb), 231.604 nm (Ni), 401.225 (Nd) and 353.170 nm (Dy). Simultaneously the screening analyses for metal ions in solid and liquid phases were performed by semi-quantitative EDX techniques (Hitachi TM-1000-μ-DEX). For each sample in EDX analyses, at least five different areas were studied, and the average value was calculated and given as the relative content of the elements.

#### 2.10.2. Batch sorption experiments

Batch sorption experiments were performed at room temperature under optimal pH conditions in a shaker incubator at 150 rpm for 1 h, using plastic tubes containing 3–10 mL of working solution and 0.025–0.25 g of the adsorbents. The pH of the solution was adjusted by using 0.1 mol $L^{-1}$ HCl or NaOH and without adding any buffer to control the pH consistently. After a period of agitation (overnight), the suspensions were filtered to collect the final solutions.

*Adsorption isotherms.* The adsorption isotherms were studied by varying the initial metal concentrations from 10 to 400 mg $L^{-1}$ with 0.05 g of adsorbent and 20 mL of metal solution, applying shaking overnight at room temperature with controlled suspension pH.

The adsorbed metal amount was determined by the difference between initial and final metal concentrations in the solution using the following equation:

$$q_e\left(mg \cdot g^{-1}\right) = \frac{(C_0 - C_e) \cdot V}{m} \quad (1)$$

where $q_e$ is the amount of metal adsorbed per mass unit of adsorbent at equilibrium ($mg \cdot g^{-1}$); $C_0$ and $C_e$ are the initial and equilibrium concentrations of the metal ions ($mg \cdot L^{-1}$), respectively; $V$ is the volume of the solution (L), and $m$ is the weight of the solid (g).

The effects of various parameters on the adsorption capacity of both functionalized and non-functionalized SBA-15 in the experiments were also investigated.

#### 2.10.3. Metal ion recovery as a function of pH

The adsorption of Fe(III), Ni(II), Cu(II), Pb(II), Cr(III), Ca(II), Nd(III) and Dy(III) ions on adsorbent as a function of solution pH was studied for a set of experiments using 50 mg of adsorbents dispersed in 20 mL of metal-containing solution with concentration $10^{-4}$ mol $L^{-1}$ having different pH in the range of 1.0–9.0. After 30 min of stirring, the adsorbent was separated in a magnetic field, and the metal content of the solution was determined by ICP-OES.

Metal ions recovery was calculated from the equation:

$$Recovery\ (\%) = C_0 - C_e/C_0 \cdot 100\% \quad (2)$$

#### 2.10.4. Desorption studies

Reusability of the mesoporous adsorbents for water treatment was investigated in consecutive cycles of adsorption/desorption experiments under static mode. The desorption experiments were carried out in a 5 mL of 0.1–1 M nitric acid solution for 1–12 h at room temperature with stirring on a shaker. After centrifugation at 5000 rpm for 10 min, the concentration of metals in the supernatant was determined, from which the quantitative desorption of metal ions from mesoporous samples was calculated.

## 3. Results and discussion

The synthesis of functionalized mesoporous silicas was carried out according to the scheme described in Fig. 1. The surfactant used in the synthesis (P123) as the template, forms a rod-like micelles in the strongly acidic medium. The hydrolytic polycondensation reactions of structuring (sodium silicate (SS)) and functionalizing (DPTS, APTES, APTS, EDTA) agents occur on the surface of surfactant micelles. During the synthesis of different kinds of mesoporous silica, the ratio of reagents, initial -carboxylic, -phosphonic, amine-containing alkoxysilanes, and processing mode were varied to obtain a higher mass fraction of functional groups in the final product. It is interesting to note that the effect of pH of the reaction mixture on the course of structure formation in this work was traced. All synthesized samples were fine-dispersed white powder.

### 3.1. Morphology characterization

Fig. 2 presents the morphology of the different mesoporous silicas synthesized using sodium silicate and different functionalizing agents. The particles show significant differences in sizes and shapes despite of using similar synthesis routes and sodium silicate as the reagent in all cases. The bare silica consists of short cylinders with parameters 1 × 0.5 μm, packed in long agglomerates "mustache" with a size of 10 μm or more. The SBA-NH sample also shows similar shapes but highly irregular and glutted together. SBA-EDTA exhibited a plate morphology and forms flack aggregate with specific ordering. SBA-EDTA-NH and SBA-EDTA-NH1 consist of spherical particles around 1 μm size and form aggregated clusters. SBA-EDTA-POOH1, and SBA-EDTA-POOH showed dispersed spherical particles with less agglomeration. The reason for these differences can be the effect of the pH of the reaction mixture during the formation of micelles and silica framework. The presence of a

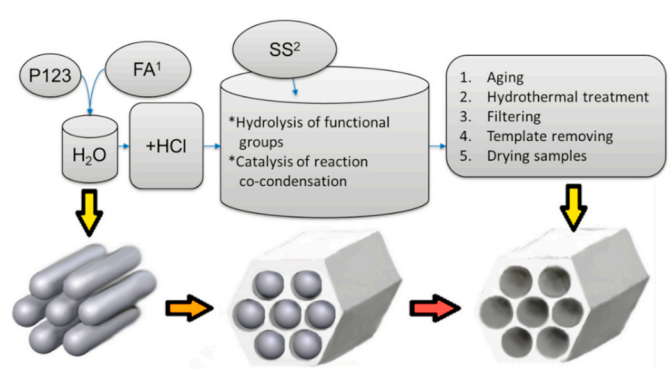


**Fig. 1.** Template synthesis of hybrid inorganic-organic mesoporous silicas (1 -FA - Functionalized alkoxysilane, 2 - SS – sodium silicate).

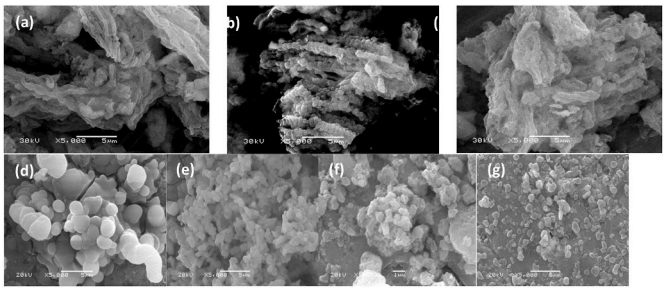


**Fig. 2.** SEM micrographs of the synthesized samples: SBA (*a*), SBA-EDTA (*b*), SBA-NH (*c*), SBA-EDTA-NH1(*d*), SBA-EDTA-NH (*e*), SBA-EDTA-POOH1 (*f*) and SBA-EDTA-POOH (*g*).

higher concentration of acidic groups caused formation of the fine particles.

Transmission electron micrograph (TEM) images further verified the results of the SEM analysis. The TEM data (Fig. 3) showed that not all samples have had a well-ordered hexagonal structure (p6mm), as we expected. The nature and ratio of reagents, as well as the size of the functionalizing groups, have a significant effect on the 2D hexagonal structure formation process. It is thus impossible to obtain materials with a high concentration of groups with the preservation of the values of structural parameters. Thus, to get a well-ordered structure of the SBA-15 type in the case of EDTA groups, their introduction was only possible at a ratio of 20:1 (Table 1), i.e., SBA-EDTA and SBA-EDTA-POOH samples, the addition of APTES and DPTS allowed synthesizing ordered materials at much higher concentrations of functionalizing alkoxysilanes. For bifunctional samples with amino and amino carboxylic (EDTA) groups, the optimal ratio was observed at 10:1:1 (Table 1), e.g. in SBA-EDTA-NH sample. These samples were used in further studies.

### 3.2. Small-angle X-ray diffraction characterization

The influence of the ratio of various components and treatment mode on the structural characteristics of the synthesized samples was investigated using XRD analysis and the corresponding data are shown in Fig. 4. The presence and location of sharp reflexes in the X-ray diffraction pattern is a fundamental factor in the classification of the materials obtained. Thus, the functionalized SBA-15-based samples with honeycomb-like hierarchical structures (see Fig. 3) were studied with XRD (Fig. 4) which showed three well-resolved typical diffraction peaks associated with a two-dimensional *P6mm* hexagonal symmetry, suggesting a highly ordered and hexagonally arranged pore system, characteristic of SBA-15 [8]. Further, one intense reflection centered approximately at $2\theta \approx 0.9$ and two very low-intensity peaks at about $2\theta$ near 1.7 and 1.5 were observed, which can be indexed as the (100),

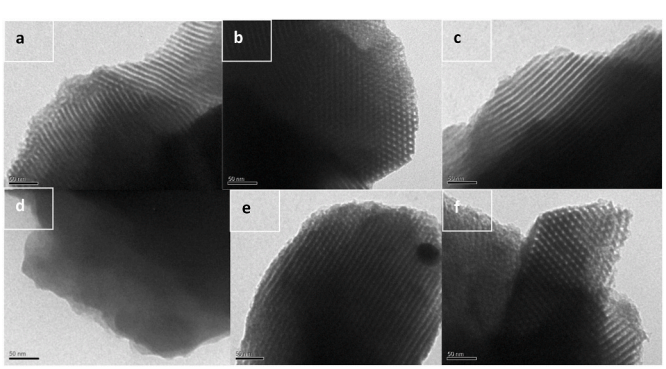


**Fig. 3.** TEM micrographs of the synthesized samples: SBA (a), SBA-EDTA (b), SBA-NH (c), SBA-EDTA-NH1(d), SBA-EDTA-NH(e) and SBA-EDTA-POOH(f).

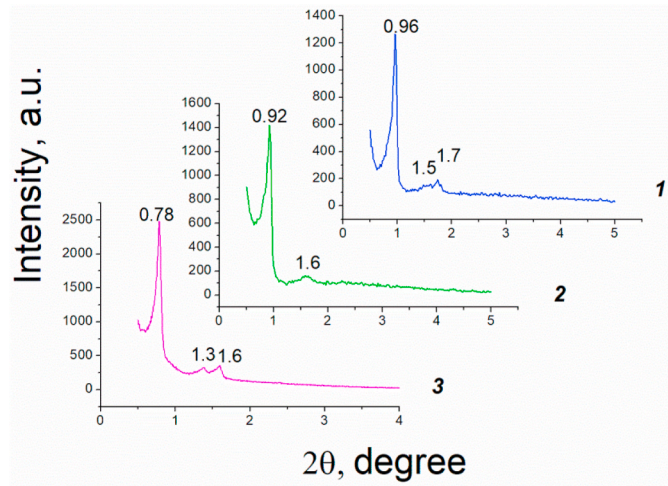


**Fig. 4.** Small-angle XRD patterns of obtained samples: 1– SBA-NH, 2 – SBA-EDTA, 3 – SBA-EDTA-POOH.

(110), and (200) hkl reflections, respectively [35]. This indicates the absence of changes in the hexagonal symmetry of the pores of the SBA-15 with the incorporation of heteroatoms containing groups. DPTS and EDTA led to formation of a material with low displacement XRD peak ($2\theta = 0.78$), indicating a robust disruptive effect of mixture of alkoxysilanes on the formation of SBA-15 mesostructure under the applied experimental conditions. The introduction of high concentrations of phosphorus-containing and amino groups lead to the deterioration of structural parameters [30]. Thus, low-angle XRD patterns further verified the results of TEM observations.

### 3.3. Porous structure characterization

The textural properties of the bare and organo-functionalized mesoporous SBA-15 were studied by $N_2$ adsorption/desorption isotherms at 77 K. The isotherms of synthesized samples along with pore distribution curves are shown in Fig. 5. All samples exhibited irreversible Type-IV adsorption-desorption isotherms according to the IUPAC classification [36] with an S-shaped (H1-type) hysteresis loop in the partial pressure range from 0.55 to 0.80, which is characteristic of SBA-15 materials with 6–8 nm pore diameter (Fig. 5 insert) [37]. A well-defined step occurs approximately at $p/p_0$ near 0.6, which is associated with the filling of the mesopores due to capillary condensation. The amount of adsorbed

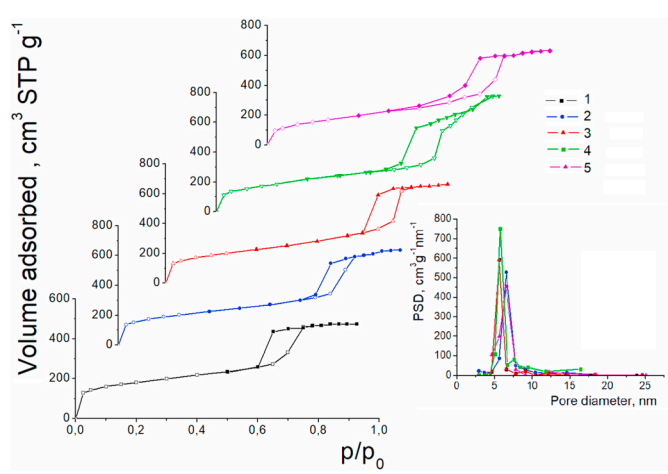


**Fig. 5.** $N_2$ adsorption/desorption isotherms and pore distribution (inset) of mesoporous samples: 1- - SBA (pure), 2 – SBA-NH, 3 – SBA-EDTA-NH, 4 – SBA-EDTA, 5 – SBA-EDTA-POOH.

$N_2$ increases and the inflection point of the step shifts from 0.7 to 0.55 value of relative pressure for functionalized SBA-15 materials. An increase in the volume of adsorbed $N_2$ compared to pure SBA-15 suggests that the structure is formed with the participation of not only sodium metasilicate but also trifunctional silanes. This is an unexpected effect and atypical for functionalized materials obtained by grafting [13]. Indeed, the sorbent isotherm based on SBA-15 shows a one-step desorption branch, indicating the existence of an open-pore structure. Based on the works of Van der Woort [38,39] we suggested that the appearance of micropores in the samples is due to channels in the walls of mesopores. In some reports it is indicated that if the temperature of formation of the mesostructure is below 130 °C, then a high contribution of micropores will be recorded, which can be formed both in the wall of mesopores and due to the hierarchical structure formed by tri-functional alkoxysilanes [40,41]. However, in our case, a small fraction of micropores (till 2 nm) was identified, although at all stages of processing the temperature did not exceed 80 °C (Fig. S1). It is possible that in our methods, the influence of the nature of functional silane was more significant than that of the temperature. Using these isotherms, the parameters of the porous structure of the obtained samples were calculated (see Table 2). Significant increase in the textural parameters, such as surface area and total pore volume, of the organically functionalized samples, indicate an open-pore structure produced by functionalization. The formation of rod-shaped SBA-15 materials with uniform and narrow pore size distributions with sizes ranging between 5.7 and 8.2 nm were confirmed according to DFT calculation [33,34].

Nevertheless, the pore size distribution of the SBA-EDTA sample calculated from the adsorption branch of the isotherm is bimodal and relatively broad with the maximum shifted to 20.6 nm as compared to other samples. This behavior shows that the ordering of the pores in SBA-EDTA sample has increased due to influence of the size of the functional group on the structure-forming process. Maybe these pores were additionally formed between ethylenediaminetriacetic groups. Here it is important to note for comparison that the bi-functional SBA-EDTA-POOH samples showed the same effect with maximum second pore size at 19.7 nm (Fig. 5).

### 3.4. Thermogravimetric analysis

Thermal analysis of the obtained material was performed to examine its decomposition and thermal characteristics (Fig. 6). The TG curves of the samples indicate a significant weight loss, which starts immediately with the increase of the temperature. Compared with 9.2% weight loss of the SBA15 sorbent recorded during heating from room temperature to 800 °C, the SBA-EDTA-NH, SBA-EDTA, SBA-EDTA-POOH, and SBA-NH samples exhibit weight losses of 29.1%, 27.3%, 19.3%, and 18.0%, respectively. It clearly shows that in the first case, there is no intense peak after 100 °C, which commonly appears due to evaporation of the physically adsorbed water and solvent [42]. It can be seen from this figure that traces of extractant and adsorbed water are removed up to 120 °C (8% for SBA, 10% - SBA-EDTA-NH, 12% - SBA-EDTA, 5% -SBA-EDTA-POOH, 5% - SBA-NH). The effectiveness of removing the template from mesophases with acidified ethanol is confirmed by the absence of such a peak in the samples except for SBA-EDTA-POOH and SBA-EDTA-NH.

**Table 2**
Textural parameters of obtained mesoporous samples.

| Sample | $N_2$ desorption isotherms | | | | XRD analysis | | |
|---|---|---|---|---|---|---|---|
| | $S_{BET}$, $m^2 g^{-1}$ | $V_{total}$, $cm^3 g^{-1}$ | [1]d, nm | [2]d, nm | d, nm | $h_w$, nm | $a_0$, nm |
| SBA-15 | 616 | 0.73 | 5.6 | 5.7 | NA | NA | NA |
| SBA-EDTA | 733 | 1.00 | 6.6 | 6.0 | 9.7 | 1.4 | 11.1 |
| SBA-NH | 700 | 0.99 | 6.6 | 6.0 | 9.2 | 1.4 | 10.5 |
| SBA-EDTA-NH | 710 | 1.03 | 6.6 | 8.2 | NA | NA | NA |
| SBA-EDTA-POOH | 633 | 0.97 | 6.6 | 8.0 | 11.3 | 1.7 | 13.1 |

Notes: 1 – calculated by the BJH method [32], 2 – MND method [33,34], N/A – not available.

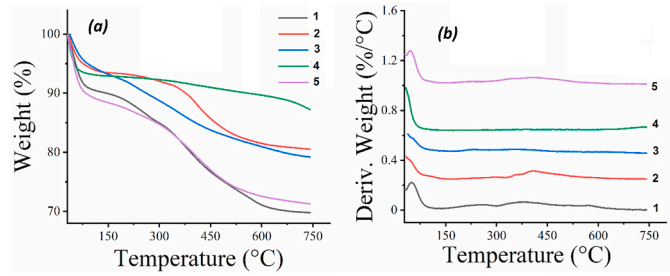


**Fig. 6.** TGA (a) and DTG (b) curves of SBA-EDTA-NH (1), SBA-NH (2), SBA-EDTA-POOH (3), SBA (4), and SBA-EDTA (5) synthesized mesoporous samples.

The decomposition of the organic component can be observed in the temperature range 300–500 °C (5% for pure silica; 13% for SBA-EDTA-POOH and SBA-NH samples; and ~18% for SBA-EDTA-NH and SBA-EDTA samples). The more considerable weight loss in SBA-EDTA-POOH and SBA-NH samples with respect to SBA-EDTA-NH and SBA-EDTA samples can be attributed to the introduction of more functional groups into SBA-15. The presence of the peak showing mass loss at the level of 3% in the region of 500–700 °C can be resulted due to the compaction of the structure leading to the change in the heat capacity of the sample. For SBA-EDTA-NH the weight loss comes presumably from silanol condensation. This is seen in Fig. 3, where an amorphous component is present. SBA-EDTA and SBA-NH samples also exhibit a large peak with low intensity between 200 and 300 °C, which could be explained by loss of some oligomeric structure from the surface. Thus, the results of the thermogravimetric analysis confirmed the presence of the functional groups on the SBA-15 surface. Those groups have high thermal stability (above 300 °C), suggesting that the SBA-15 silica samples have application prospects for use at relatively elevated temperatures.

### 3.5. Fourier transform infrared (FT-IR) analysis

The chemical structure of mesoporous materials was further verified by FT-IR spectroscopy and the data are shown in Fig. 7. The FT-IR spectra obtained for all synthesized materials contained in the region 1050-1150 $cm^{-1}$ the most intense absorption band, which usually has a shoulder from higher frequencies. The appearance of this band is typical for the three-dimensional framework of the siloxane bonds ≡*Si*–O–Si [43]. In the region of 2800–3000 $cm^{-1}$, there are absorption bands characteristic of the valence oscillations of the C–H bonds. The spectra of carboxyl-containing silicas are very similar. The absorption bands in the region of 1716–1724 $cm^{-1}$ confirm the presence of COOH group [44]. A medium intensity band in the region of 1409–1417 $cm^{-1}$ is associated with the oscillation of the $\nu((Si)CH_2)$ propyl fragment. In all samples with amino- and aminocarboxylic groups, the $\nu$(C–N) band, which generally appears around 1250−1010 $cm^{-1}$, cannot be observed, since it overlaps with the saturated $\nu_{as}$ (Si–O–Si) bond of the SBA-15 matrix. Most of the obtained samples contained some isolated silanol groups manifested by $\nu$(OH) at 3750 $cm^{-1}$, adjoined by the broad absorption band at 3200−3600 $cm^{-1}$ corresponding to water-bonded OH-groups. After amino-functionalization, regardless of the co-condensation, the absorption band characteristic of isolated silanol groups did not increase but even decreased for SBA-EDTA-POOH compared to that of bare SBA-15. This is an indication of the interaction between silanol group and the functional groups of the SBA-EDTA-POOH sample. The presence of characteristic bands at 1215 $cm^{-1}$ from the P═O groups vibration in phosphonic acid in the SBA-EDTA-POOH adsorbent confirmed their efficient including into mesoporous matrix.

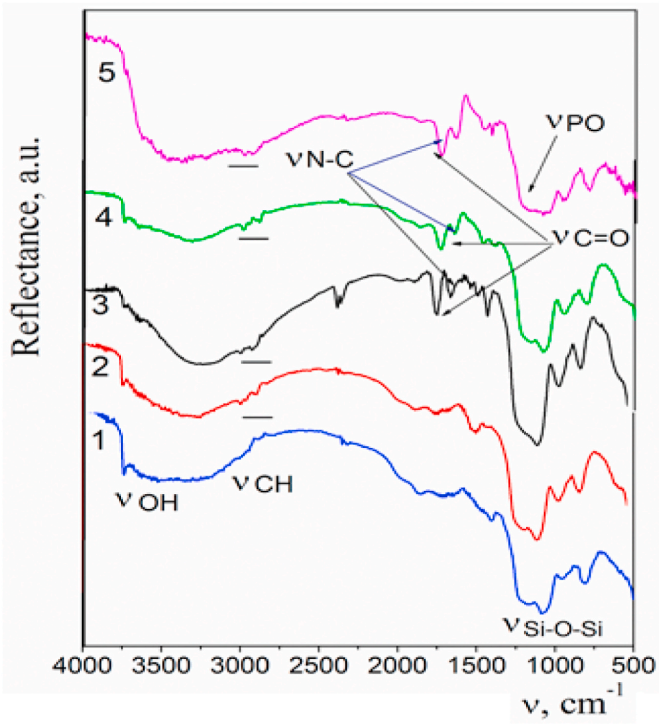


**Fig. 7.** FT-IR spectra of SBA (1), SBA-NH (2), SBA-EDTA-NH (3), SBA-EDTA (4) and SBA-EDTA-POOH (5) samples.

### 3.6. Concentration of functional groups in silica

The concentration of different functional groups present on SBA-15 after functionalization was estimated using CHN analysis. The data presented in Table 3 clearly shows the presence of nitrogen in $NH_3^+$- and EDTA functionalized materials and also confirms the efficiency of the introduction of N-containing functional groups by the developed method. The results of also indicate that the monofunctional samples contained more than 1.75% of nitrogen, whereas in case of bi-functional groups, the N-content was decreased significantly. Thus, the functional group's amount for obtained samples was verified in a wide range from 0.32 mmol $g^{-1}$ to 1.26 mmol $g^{-1}$. The higher amount of functional groups (1.27 mmol $g^{-1}$) was typical of the ammonium functionalized SBA-15 sample.

For comparison with the elemental analysis, the total content of acid and base groups were further evaluated by acid-base potentiometric titration, which has been widely used to determine the amounts of acidic and basic surface groups in functional materials [45]. This approach was employed to quantify the amounts of specific carboxyl, ammonium, and phosphonic groups present in the functionalized silica samples (Fig. S2). Different numbers of endpoints were observed in mono- and bi-functional materials. For instance, the titration curves of SBA-EDTA-NH and SBA-EDTA-POOH samples exhibited two endpoints. From the amounts of NaOH titrated in each stage, the amounts of the specific functional groups in the materials were calculated and summarized in Table 3. A comparison of functional group content for several silica samples measured by the elemental analysis and titration assay is also shown in Table 3. As noted above, the two assays give correlating results for some samples, with up to ~70% lower amine content estimated for the SBA-NH samples using the titration method. The elemental analysis routinely measures a higher total amine content than titration assay substantiating our earlier conclusions [45] that silica modified with APTES has inaccessible amino groups. We had hypothesized that the higher total amine content was due to the localized regions of amine multilayers or blocking in pores that are not accessible to reagents during the titration assays. As a result, these are not accessible for adsorption.

For adsorbents in an aqueous medium, it is important to study electrokinetic potential for suspensions in a wide range of pH (Fig. S3). The effect of an increase in the pH on the electrokinetic potential of modified samples is characterized by a slight increase in the negative ζ value, followed by a significant decrease in its absolute value (Fig. S3). The general trend is a substantial rise in the absolute (negative) value of zeta potential with increasing pH, from about 15 mV at pH 2 to −20-(-40) mV at pH 8–10. This is due to the increasing dissociation of different kinds of functional groups having different degree of dissociation: initial Si–OH groups, weakly charged –COOH, and moderately charged $–NH_3^+$ and POOH groups. A decrease in zeta potential at pH < 2 and pH > 10 can be due to the increase in the ionic strength of the solution (>$10^{-2}$ M of HCl or KOH, respectively) accompanied by the electrical double layer compression. Recharging for a sample containing an amino group in the surface layer occurs at neutral pH, which logically and additionally confirms their presence and availability for adsorption interactions (see details [46,47]). The presence of carboxyl groups reduces the zeta potential of the surface of mesoporous silica, which facilitates the sorption of organic molecules [48].

**Table 3**
The amount of functional groups for obtained samples (elemental and titrimetric analysis).

| Sample | Functional groups | Elemental analysis | | | | pH-metry |
|---|---|---|---|---|---|---|
| | | N, % | C, % | H, % | $C_L$, mmol·$g^{-1}$ | $C_L$, mmol·$g^{-1}$ |
| SBA-EDTA | -EDTA | 0.49 | 6.53 | 2.51 | 0.35 | 0.33 |
| SBA-NH | $-NH_3^+Cl^-$ | 1.74 | 9.01 | 3.05 | 1.26 | 0.11 |
| SBA-EDTA-NH | $-NH_3^+Cl^-$/-EDTA | 1.06 | 8.57 | 2.83 | 0.51/0.25 | 0.10/0.32 |
| SBA-EDTA-POOH | $-PO(OH)_2$/-EDTA | 0.37 | 0.24 | 0.86 | -/0.27 | 1.27/0.35 |

Note: $C_L$ – concentration of functional groups (or ligands).

### 3.7. Adsorption properties of obtained mesoporous materials in a single-component aqueous solution

In the series of synthesized mesoporous SBA-15 silicas with various combinations of functional groups, two samples (SBA-EDTA-POOH and SBA-EDTA-NH) with unequal textural characteristics and higher concentration of groups (please see Table 3) were selected to establish the relationship between abovementioned features of these compounds and their adsorption properties. Also, the monofunctional mesoporous silica with individual EDTA groups (SBA-EDTA) and bare SBA-15 were evaluated as model samples for elucidating adsorption sites and extraction mechanisms for removal of metals from aqueous solution. The most effective adsorbent among synthesized mesoporous samples for the removal of REEs or heavy metals was selected at optimum adsorption conditions after elucidating their nature and extraction mechanisms.

#### 3.7.1. Optimization of extraction conditions

In adsorption studies, the pH of solutions is an important parameter that determines the recovery of metal ions due to its influence on the surface properties of the adsorbent functional groups and the ionization/dissociation of the adsorbate. The monofunctional (SBA-EDTA) and bifunctional (SBA-EDTA-POOH) samples were tested for pH influence to metal ions extraction in the range of 1.0–9.0 (Fig. 8). The effect of the suspension acidity on metal ions recovery (%) on adsorbents were studied for metal concentration that is much less than the adsorption capacity. Typically, health-important Ca(II) and Mg(II) ions are the common cations present in real water that may also get quantitatively removed with target metal ions or can affect the removal of target heavy

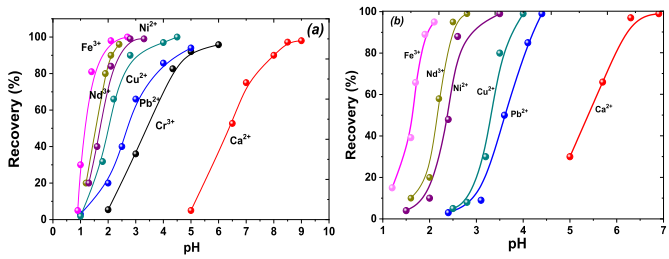


**Fig. 8.** Recovery of metal ions with SBA-EDTA (a) and SBA-EDTA-POOH (b) samples as a function of pH (Experimental conditions: $C_M = 150$ mg $L^{-1}$, V = 20 mL, m = 0.05 g, t = overnight).

or REEs ions. For this reason, all prepared adsorbents were evaluated in the pH range where Ca(II) ions interference was less.

Fig. 8 clearly confirms the relationship between recovery of metal ions and pH of the SBA-EDTA and SBA-EDTA-POOH samples suspension. For both the samples it was observed that recovery for target metals substantially decreases with increasing suspension acidity. Fe(III) ions were completely removed from the solution by adsorbents at a pH below 2.0, while adsorption of matrix ions, such as Ca(II) can be achieved only from solution with pH > 7.5. The adsorption at pH > 6.0 was not used because of precipitation due to the hydrolysis of the metal ion including REEs [49]. Quantitative recovery of Ni(II), Cu(II), and Pb(II) ions by SBA-EDTA from the solution at pH 2.0 to be about 90, 50% and 20%, respectively (Fig. 8a), while these elements demonstrated negligible adsorption on SBA-EDTA-POOH sample under above condition (Fig. 8b). The SBA-EDTA sample removes Fe(III) and Nd(III) ions under almost the same conditions (pH~1.5–2.2). Essential adsorption was observed on SBA-EDTA-POOH from REE solution under pH 2.2, while about 80% of Fe(III) can be recovered at pH ~ 2.0. It was also observed that Fe(III) and Nd(III) ions (Dy(III) also, not shown in Fig. 8b) cannot be selectively separated under above conditions using this adsorbent. Almost all studied metals (except Fe(III) ions, which precipitates at pH near 3.0), could be quantitatively removed from the solutions with 2.5 < pH < 5.0 using SBA-EDTA-POOH sample. Furthermore, all $SiO_2$-based adsorbents can only be used at pH < 8.5. Therefore these conditions were used as optimal to study the behavior of target REE ions in a single-component solution and then selective recovery of the other metals from contaminated water.

The affinity of complexing metal ions to functionalized silica described through pH value of 50% ($pH_{50\%}$) adsorption (Fig. 8), which varies as follows:

| | |
|---|---|
| *SBA-EDTA* | $Fe^{3+}(1.2) > Nd^{3+}(1.6) > Ni(1.6) > Cu^{2+}(2.0) > Pb^{2+}(3.0) > Cr^{3+}(3.8) > Ca^{2+}(7.0)$ |
| *SBA-EDTA-POOH* | $Fe^{3+}(1.5) > Nd^{3+}(2.1) > Ni^{2+}(2.2) > Cu^{2+}(3.3) > Pb^{2+}(4.0) > Ca^{2+}(5.5)$ |

It should be noted that the $pH_{50\%}$ for SBA-EDTA being consistent with stability constants of EDTA-complexes in solution [50]. The complexes stability constants of Fe(III) (logK = 18.8), Nd(III) (logK = 16.6), Dy(III) (logK = 18.3), and Cu(II) (logK = 17.8) including Pb(II) (logK = 11.3) was found to be higher than Ca(II) (logK = 10.7). Similar correlation of the adsorption efficiency versus $pH_{50\%}$ was also observed for other EDTA-containing adsorbents [51]. This indicates that the SBA-EDTA adsorbent can be employed to efficiently remove most of the metal ions from their aqueous solutions. Thus, it can be concluded that adsorption of metal ions on SBA-EDTA occurs predominantly due to the complexation with functional groups present on the adsorbent. Hence, in this case, the mechanism of metal ions adsorption on the silica adsorbents modified with EDTA groups is based on inner-sphere complexation reaction through the chelate effect combined with van der Waals interaction. Some difference in values of $pH_{50\%}$ for SBA-EDTA and SBA-EDTA-POOH can also be seen. For example, 50% recovery of Nd(III), Pb(II), and Cu(II) ions for SBA-EDTA can be accomplished from high acidic solution than for SBA-EDTA-POOH, which is attributed to the other mechanism of extraction of metal ions. This can be explained by the effect of ion-exchange phosphonic groups on the surface of the SBA-EDTA-POOH sample.

### *3.7.2. Behavior of most effective SBA-15-based adsorbents for removal of the metal ions in single-component solution*

Adsorption capacity of a material is very important feature because it determines the maximum amount of analyte adsorbed per gram of the sorbent. The batch method was used to investigate the adsorption capacity of obtained materials and the relevant data are presented in Fig. 9. The measurements were repeated for each individual metal ions separately. In order to limit the competitive equilibria for metal hydroxide formation, subsequent uptake experiments were performed at pH < 5.0, and the spectrophotometry and ICP-OES methods were used to determine the concentration of heavy metals and REEs, respectively.

The results demonstrated in Fig. 9 indicate that the adsorption capacity in an individual solution for the 4 metal ions (Fe(II), Pb(II), Nd (III), and Dy(III)) was comparatively higher than other metal ions on some of the adsorbents. It was also observed that the adsorption performance of non-functionalized SBA-15 for chosen metal ions was the lowest among the tested adsorbents, despite having large surface area (as indicated by $N_2$ adsorption/desorption data, Table 2) and the exposed silanol groups on its surface. Therefore, it can be concluded that the contribution of silanol group in the SBA-15 to the studied metal ions adsorption was significantly low. After functionalization, regardless of the type of N-containing groups (SBA-EDTA-NH and SBA-EDTA samples), the metal ions uptake was considerably increased as compared to bare SBA-15. The adsorption capacity of 1 g of SBA-EDTA was found to be 0.60 mmol for Fe(III), 0.40 mmol for Ni(II), 0.35 mmol for Pb(II), 0.39 mmol for Cu(II), 0.32 mmol for Nd(III), and 0.34 mmol for Dy(III), respectively. Fig. 9 also indicate that the adsorption capacity of metal ions increased with the total functionality on silica. Among differently functionalized materials, SBA-EDTA-POOH silica possesses higher adsorption capacity than other bifunctional group containing samples (e.g., SBA-EDTA-NH). Considering that the SBA-EDTA-NH adsorbent shows a similar ability of metals removal as its SBA-EDTA counterpart, the optimum capacity of SBA-EDTA-POOH for adsorption of heavy metals was found to be within the range pH 4.5–5.0. After the adsorption study, it becomes clearly noticeable that the most effective binding of Fe (III) ions occurs on –EDTA/-phosphonic group containing samples. In

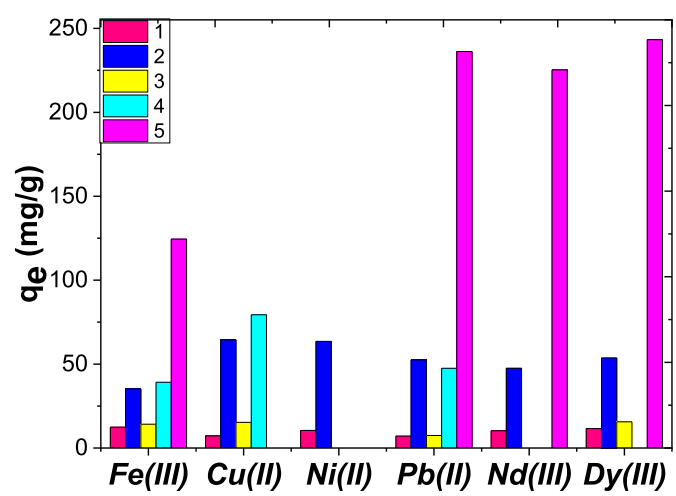


**Fig. 9.** The adsorption capacity of neat and functionalized materials for individual metal ion solutions (200 mg $L^{-1}$, adsorbent dose: 0.025–0.030 g, suspension volume 20 mL, pH: 2.2–2.4 for Fe(III), 4.5 for Cu(II), Pb(II) and Ni(II) at room temperature) SBA (1), SBA-EDTA (2), SBA-NH (3), SBA-EDTA-NH (4), and SBA-EDTA-POOH (5) samples.

order to eliminate the interfering effect of Fe(III), it is advantageous to remove it by precipitation using solutions with controlled pH. According to $S_{BET}$ result of SBA-EDTA-POOH (633 $m^2$ $g^{-1}$, Table 2), an average coverage of 2.56 functional groups μmol/$m^2$ (1.27 mmol $g^{-1}$ (-PO$(OH)_2$) + 0.35 mmol $g^{-1}$ (-EDTA) = 1.62 mmol $g^{-1}$ = 2.56 μmol $m^{-2}$) along with a distance between two groups of more than 1.6 nm was calculated. This shows that the distance between two functional groups is quite large that single metal ion cannot interact with two or more functional groups at the same time. This reveals that molar ratio $C_L$: M = 1:1 can be an exclusive complexation condition on the SBA-EDTA-POOH adsorbent. Similarly, the SBA-EDTA-NH and SBA-EDTA adsorbents which possess even lower functional groups concentration and with high $S_{BET}$ can also be characterized by the same ratio on the surface complex formation.

The values of maximum adsorption capacity for the metal ions in single component systems were in good agreement with concentration of functional groups in adsorbent as obtained by elemental analysis and pH-titration (Table 3). At least four functional groups, which possess donor properties, are spatially arranged in such a way that they can usually form 1:1 complexes [52]. In this way, five- or six-membered rings can be formed with various metal ions having two or three charges. The difference in the adsorption capacities of Nd(III) and Dy (III) ions by SBA-EDTA-POOH silica are almost tenfold than the unmodified SBA-15. The adsorption capacity for REEs follows an increasing trend in the order of SBA < SBA-EDTA < SBA-EDTA-POOH. The SBA-EDTA-POOH silica yielded the best adsorptive removal of REEs from the solution in absence of any other interfering metal ions. The mechanism of adsorption of any species onto mesoporous adsorbents can comprise two stages: (a) migration of the species from bulk solution to the boundary layer surrounding the mesoporous silica and (b) adsorption based on complexation of the species in the pores or at the active sites of the adsorbent.

For REEs such as Nd(III) and Dy(III), an equilibrium between complexes with coordination numbers 9 and 8 are expected [51,53,54], whereas for cations such as Cu(II), Ni(II), and Fe(III) the coordination number is 6, which is preserved due to the inclusion of water molecules. The peculiarity of EDTA lies in the fact that this ligand is characterized by mixed ligand (the inner sphere of which includes at least two types of ligands without considering the solvent), which forms bi-nuclear (or bimetallic) and hetero-nuclear complexes. The amount of the adsorbed Nd(III) (1.64 mmol $g^{-1}$) equals the concentration of functional groups on these samples (0.33 mmol $g^{-1}$ (SBA-EDTA) and 1.27/0.35 mmol $g^{-1}$ (SBA-EDTA-POOH), Table 3). Therefore, REEs are initially adsorbed by -PO$(OH)_2$/-EDTA groups to form 1:1 complexes ($\equiv Si–(CH_2)_2–P(O)(OH)_{2(s)} + Nd^{3+}{}_{(l)} \leftrightarrow \equiv Si–(CH_2)_2–P(O)O_2Nd^{+}{}_{(s)} + 2H^{+}{}_{(l)}$) during which in addition to phosphonic acid groups the chelating groups can also form complexes. In the second stage, in presence of high metal ions concentration, the formation of 1:1 complex with EDTA-groups or hetero-ligands complexes was observed. Thus, 1:1 complex should occur predominantly in the surface of SBA-EDTA-POOH sample as schematically presented in Scheme 1.

The molar ratio of adsorbed REEs to functional group of adsorbents, complexes of 1:1 composition are formed, while for heavy metals, the formation of complexes 0.5:1 is only possible. Apparently, the coordination sphere of the Fe(III) ion includes two phosphonic groups, while the coordination spheres of Nd(III) and Dy(III) ions include only one bidentate phosphonic group along with several EDTA residues. The central atom in the REEs complexes requires a high coordination number, which may lead to the formation of coordination unsaturated complexes on the surface of mesoporous silica. It is also highly likely that some solvent molecules can occupy free coordination sites or other ligands (in the form of impurity) present in the system, such as dyes. This indicates that the formation of heteroligand complexes is possible on the surface.

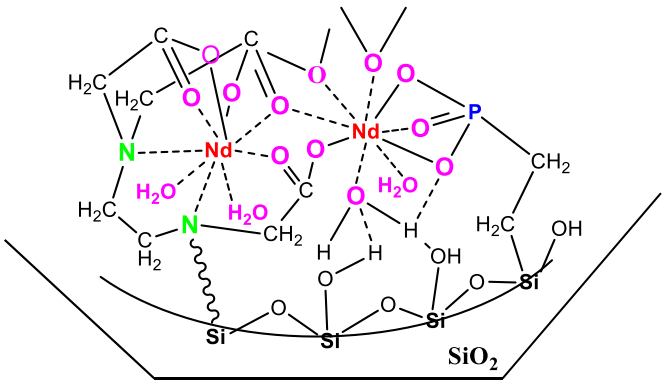


**Scheme 1.** Possible structure of the Nd(III) complex in the SBA-EDTA-POOH sample.

### 3.7.3. Adsorption isotherms

From an overall perspective, the effect of functionalization of mesoporous silica on their efficiency in the REEs uptake was investigated by considering distinct types of surface donor atoms (O, N, P) available for adsorption in most attractive modified SBA-15-based adsorbents such as SBA-EDTA and SBA-EDTA-POOH. Affinity and capacity of SBA-EDTA and SBA-EDTA-POOH samples towards target REEs were evaluated from the adsorption isotherms of Nd(III) and Dy(III) ions (Fig. 10).

The adsorption capacity for these equilibrium concentration range of Dy(III) ions was higher than for Nd(III) ions for both samples at room temperature. The highest value of the Dy(III) adsorption capacity was obtained for SBA-EDTA-POOH sample. The slope of initial part (≤50 mg $L^{-1}$) of the isotherm indicates the degree of affinity of the adsorbent to the analyte. The higher slope of the isotherm inclination shows the higher analyte's affinity for the adsorbent. As it can be seen from Fig. 10, SBA-EDTA-POOH sample has high affinity to both the investigated REEs and quantitatively extracted metal ions from aqueous solution. Further, for quantification study, the above obtained isotherms were fitted with Langmuir and Freundlich isotherm models (Fig. S4, Table 4). It can be seen that both models reasonably match with the experimental adsorption data. The adsorption behavior of SBA-EDTA-POOH sample towards Nd(III) and Dy(III) is well fitted by Langmuir model with $R^2$ close to 1.00 which also confirm our hypothesis that REEs were adsorbed through complexation with the phosphonic groups on the surface of adsorbent. The $R^2$ value obtained for Freundlich model indicated that the model is not acceptable to describe the adsorption behavior of the REEs on the modified silica samples. An exception that based on the high coefficient of correlation, Freundlich model fitting like as Langmuir for Dy(III) on SBA-EDTA, which implicates the possibility of heterogeneous binding sites and multilayer adsorption.

Comparison of the obtained adsorbents with those reported in several earlier studies on adsorption of REEs and heavy metals, showed that the present method produces higher capacity than the majority of

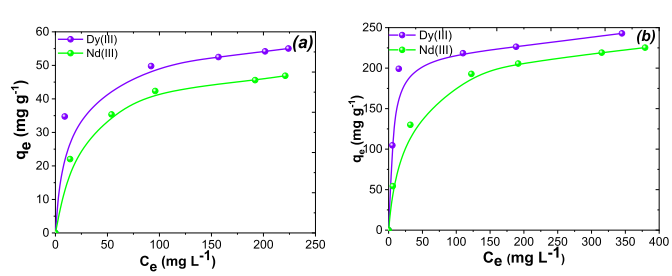


**Fig. 10.** Adsorption isotherms of Nd(III) and Dy(III) ions on SBA-EDTA (a) and SBA-EDTA-POOH (b) (Experimental conditions: 10–400 mg $L^{-1}$, adsorbent dose 0.05 g, contact time - overnight, suspension volume 20 mL, pH: 3.5 at room temperature).

**Table 4**
Summary of equilibrium isotherm parameters of SBA-EDTA and SBA-EDTA-POOH–3 samples by Langmuir and Freundlich models [55].

| Model | Parameter | SBA-EDTA | | SBA-EDTA-POOH | |
|---|---|---|---|---|---|
| | | Nd(III) | Dy(III) | Nd(III) | Dy(III) |
| Experimental data | $q_e$, (mg·g$^{-1}$) | 47.52 | 53.62 | 225.3 | 243.25 |
| Langmuir | $K_L$ (L·μg$^{-1}$) | 0.05 | 0.12 | 0.04 | 0.11 |
| $\frac{C_e}{q_e} = \frac{1}{q_m}C_e + \frac{1}{q_m K_L}$ | $q_m$ (mg·g$^{-1}$) | 51.02 | 56.50 | 238.10 | 243.90 |
| | $R^2$ | 0.9993 | 0.9987 | 0.9993 | 0.9984 |
| Freundlich | $K_F$ (mg$^{1-1/n}$ L$^{1/n}$·g$^{-1}$) | 11.25 | 25.50 | 33.85 | 96.76 |
| $\ln q_e = \frac{1}{n}\ln C_e + \ln K_F$ | 1/n | 0.2732 | 0.1433 | 0.3376 | 0.1679 |
| | $R^2$ | 0.9605 | 0.9961 | 0.9462 | 0.7441 |

reported earlier (Table 5).

### 3.8. Application of the adsorbent for analysis of the multi-component aqueous solution

The developed adsorbent was applied for the extraction of ions from the model mixture of REEs, heavy metals, and interfering ions containing Fe(III), Ni(II), Al(III), Nd(III), Dy(III) in the water solution, to analyze the effectiveness of competitive preconcentration of REEs by the synthesized adsorbents. Determination of REEs in such samples is complicated not only from the point of instrumental measurement but also from the separation of metal present in various concentration levels. Extraction of metal ions from other elements can be used to all method usually applying to solid-state sample, for example, X-ray fluorescence spectrometry or EDX. In our study, the adsorbent efficiency was estimated by semi-quantitative EDX techniques on solid-state and dried solution residues to elucidate the distribution of ions (Fig. 11). In addition, the target ions in the solution were also determined by UV–vis spectrophotometry and ICP-OES (depending on the metal concentration level). REEs present at trace level was determined by ICP-OES method with a pre-concentration step followed by elution. The data presented in Fig. 11 indicate that despite the increased affinity of the phosphonic groups for REEs ions, in an acidic solution, iron binds more actively by the SBA-EDTA-POOH sorbent under the present experimental conditions (Fig. 11).

Usually, mesoporous silicas demonstrate excellent stability in acid media [69]. Indeed, SBA-EDTA and SBA-EDTA-POOH samples do not adsorb metal ions from a solution with pH $\leq$ 1.0 (see Fig. 8). Thus, it was experimentally proved that complete desorption of metals is observed by treating the metal-containing adsorbent with 0.1 mol L$^{-1}$ $HNO_3$ for 6 h under stirring condition only for bare SBA-15 (and more than 95% by using 0.05 M EDTA).

Fig. 12 shows the effectiveness of adsorption/desorption processes for as-prepared SBA-EDTA-POOH adsorbent. Obtained results for SBA-EDTA and SBA-EDTA-POOH samples demonstrated that 99.06% of the adsorbed metal ions were quantitatively desorbed from the loaded matrix to the suspending medium using 0.5–1.0 M $HNO_3$ in the duration of 6–12 h. The increasing concentration of acid has decreased the reaction time to 6 h. The second and third adsorption cycles reveal that the SBA-EDTA and SBA-EDTA-POOH can be reused with very low loss in efficiency (4–5%). The principle of extraction of cationic and anionic forms of metals due to the combination of chelating and anion exchange centers of binding within same material with high structural and sorption characteristics actualizes obtaining highly efficient multi-functional adsorbents with predetermined properties.

## 4. Conclusions

In this study, the ability of mesoporous SBA-15 materials, unmodified and modified by grafting various combinations of

**Table 5**
Comparison of practical features of present research and several reported methods for the determination of REEs and heavy metals.

| Adsorbent | Target ions | Adsorption performance: capacity | Ref |
|---|---|---|---|
| $SiO_2$ and MNPs* with EDTA, DTPA, TTHA acids** | $Dy^{3+}$, $Nd^{3+}$, $La^{3+}$ | $SiO_2$-EDTA: 213.9 ± 9.5 mg g$^{-1}$ (Nd), 300.4 ± 10.3 (Dy); MNP-EDTA: 208.5 ± 8.6 mg g$^{-1}$ (Nd), 269.9 ± 9.5 mg g$^{-1}$ (Dy); $SiO_2$-DTPA: 299.9 ± 8.2 mg g$^{-1}$ (Nd), 168.6 ± 6.5 mg g$^{-1}$ (Dy); MNP-DTPA: 292.9 ± 7.5 mg g$^{-1}$ (Nd), 186.9 ± 5.9 mg g$^{-1}$ (Dy); $SiO_2$-TTHA: 219.9 ± 5.9 mg g$^{-1}$ (Nd), 173.3 ± 5.7 mg g$^{-1}$ (Dy); MNP-TTHA: 213.1 ± 5.8 mg g$^{-1}$ (Nd), 164.2 ± 5.2 mg g$^{-1}$ (Dy) | [53] |
| EDTA-chitosan | Ni(II) | 71 mg g$^{-1}$ | [56] |
| Amine-modified SBA-15 | Cu(II), Ni(II), Zn(II) | 43.59 mg g$^{-1}$ (Cu), 42.25 mg g$^{-1}$ (Ni) and 30.66 mg g$^{-1}$ (Zn) | [57] |
| KIT-6/EDTA | Cu(II), Ni(II), Cd(II) Pb(II) | 1.21 mmol g$^{-1}$ (Cu) 1.12 mmol g$^{-1}$ (Ni), 1.40 mmol g$^{-1}$ (Cd), 0.92 mmol g$^{-1}$ (Pb) | [58] |
| SBA-15/EDTA | Cu(II), Ni(II), Cd(II) Pb(II) | 1.35 mmol g$^{-1}$ (Cu), 1.14 mmol g$^{-1}$ (Ni), 1.07 mmol g$^{-1}$ (Cd), 1.33 mmol g$^{-1}$ (Pb) | [58] |
| Mercapto and amine-mercapto-functionalized silica xerogels | Pb(II), Cu(II) | 125 mg g$^{-1}$ (Pb), mg·g$^{-1}$ (Cu) | [59] |
| Nano $TiO_2$ | Pb(II), Cd(II), Ni(II) | 15.3 mg g$^{-1}$ (Zn), and 7.9 (Cd) mg·g$^{-1}$ | [60] |
| ETS-10 Titanosilicate | Yb(III), Nd (III), Eu(III), Tb(III), Dy (III), Ni(II) | 0.5491 mmol g$^{-1}$ (Yb), 0.4723 mmol g$^{-1}$ (Nd), 0.6519 mmol g$^{-1}$ (Eu), 0.7206 mmol g$^{-1}$ (Tb), 0.7549 mmol g$^{-1}$ (Dy), 0.5731 mmol g$^{-1}$ (Ni) | [61] |
| Strongly Acidic Cation Exchange Resin | La(III), Nd (III) | 33.55 mg g$^{-1}$ (La), 17.30 mg g$^{-1}$ (Nd) | [62] |
| PEI-$Fe_3O_4$ | Cu(II), Zn(II) | 157.8 mg g$^{-1}$ (Cu), 105.2 mg g$^{-1}$ (Zn) | [63] |
| Cellulose nanocrystals | Dy(III) | 22.57–34.03 mg g$^{-1}$ | [64] |
| Acid-treated CS-CNTs*** | Pb(II) | 158.7 mg g$^{-1}$ | [65] |
| MPTS-CNTs/$Fe_3O_4$ | Pb(II) | 65.40 mg g$^{-1}$ (at pH 6.5) | [66] |
| Graphene oxide-based nanomaterials | Cu(II) | 47 mg g$^{-1}$ | [67] |
| Zeolites | Cu(II). Pb(II), Ni(II), Zn(II), Cd(II), Cr(III) | 2.9–101.7 mg g$^{-1}$ (Cu), 10–228 mg g$^{-1}$ (Pb), 2–132.1 (Ni), 3.1–41 mg g$^{-1}$ (Zn), 2.9–129.0 mg g$^{-1}$ (Cd), 3.5–83.2 mg g$^{-1}$ (Cr) | [68] |
| SBA-15/-$PO(OH)_2$ | $Nd^{3+}$, $Dy^{3+}$, $UO_2^{2+}$ | 85 mg g$^{-1}$ (Nd), 120 mg g$^{-1}$ (Dy) | [22] |
| SBA-15/benzene triamido-tetraphosphonic acid | $Nd^{3+}$ | 129.8 mg g$^{-1}$ (Nd), pH = 6 | [19] |
| Xerogel/-$PO(OH)_2$ | $Dy^{3+}$ | 0.30 mmol g$^{-1}$ (47.3 mg g$^{-1}$) | [20] |
| SBA-EDTA SBA-PO(OH)-EDTA | Fe(III), Ni(II), Cu(II), Pb(II), Nd(III), Dy (III) | 35.2 mg g$^{-1}$ (Fe), 63.5 mg g$^{-1}$ (Ni), 52.5 mg g$^{-1}$ (Pb) and 74.4 mg g$^{-1}$ (Cu), 51.02 mg g$^{-1}$ (Nd), 53.62 mg g$^{-1}$ (Dy) 124.5 mg g$^{-1}$ (Fe), and 236.2 mg g$^{-1}$ (Pb) 236.20 mg g$^{-1}$ (Nd), 243.25 mg g$^{-1}$ (Dy) | This work |

Notes. *MNPs – magnetic nanoparticles; **EDTA - ethylenediaminetetraacetic acid, DTPA – diethylenetriaminepentaacetic acid, and TTHA – triethylenetetraminehexaacetic acid. ***CNTs – carbon nanotubes.

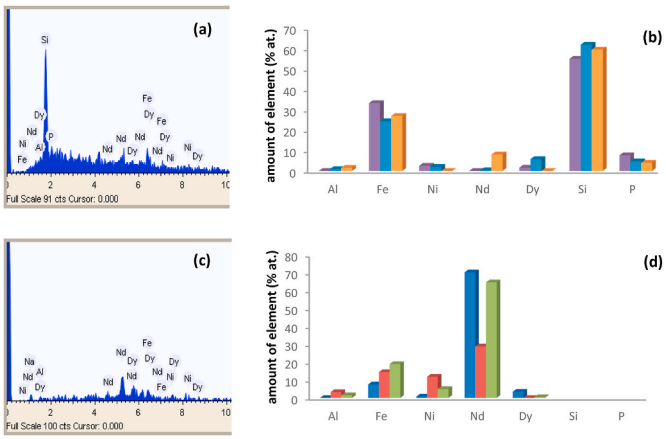


**Fig. 11.** EDX wide-scan spectrum (a, c) and elemental analysis (b, d) of SBA-EDTA-POOH adsorbent (a, b) and solution (c, d) after metal adsorption from a multi-element mixture containing Fe/Ni/Al/Nd/Dy ions.

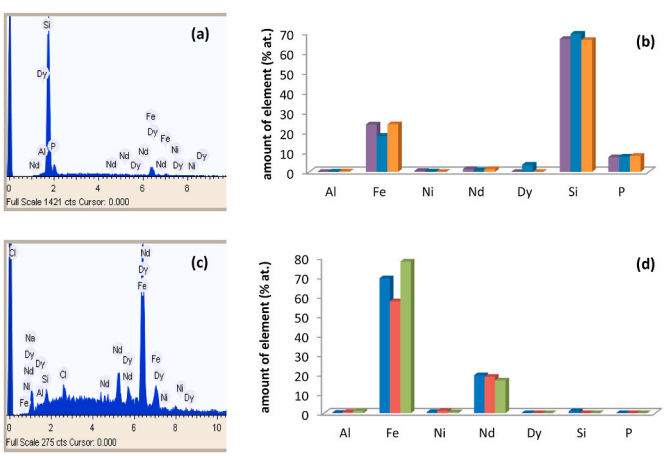


**Fig. 12.** EDX wide-scan spectrum (a, c) and elemental analysis (b, d) of SBA-EDTA-POOH adsorbent (a, b) and solution (c, d) after metal desorption from the multi-element mixture containing Fe/Ni/Al/Nd/Dy ions.

ethylenediaminetriacetic, phosphonic, protonated amino groups to remove metal ions from individual and mixture solutions was investigated by batch technique. It was observed that:

(1) The newly produced mesoporous material retained its structure properties, i.e. the highly ordered and enhanced surface area (up to 733 $m^2\ g^{-1}$) that can incorporate higher content of functional groups;
(2) The optimum pH value for the removal of Fe(III), Ni(II), Cu(II), Pb(II), Cr(III) ions by EDTA-functionalized SBA-15 material from the aqueous solutions ranging from 2 to 5. The mechanism proposed for metal adsorption on the silica adsorbents modified with EDTA groups was probably involves chelate effect and electrostatic interaction of metal ions with surface groups;
(4) The maximum adsorption capacity for most of the synthesized adsorbents was observed for Fe(III) ions. The interfering effect of Fe(III) was eliminated by precipitation with a basic solution (NaOH or $NH_4OH$).
(5) The highest adsorption capacity for heavy metals at pH 4.5–5.0 (for example, reached to 246.95 mg $g^{-1}$ for Pb(II)) was achieved with the bi-functional adsorbent containing -$PO(OH)_2$/-EDTA groups, because it retained high specific surface area and high concentration of availed functional groups;
(6) Under the optimal conditions (pH ≈ 3.5) without excess of heavy metals, the REEs (Dy(III), Nd(III), etc.) were separated by the bi-functional adsorbent with -$PO(OH)_2$/-EDTA groups from a complex mixture. The highest value of the adsorption capacity for REE was reached 238.10 mg $g^{-1}$ for Nd(III) and 243.90 mg $g^{-1}$ for Dy(III) ions. The highest value of the Dy(III) adsorption capacity could be explained in terms of the high affinity of P-containing adsorbents towards smaller Dy(III) ions and high complexation constants with chelating EDTA-groups.
(6) All metal ions, without exceptions, were successfully desorbed by 0.5–1 M $HNO_3$ (reaction time above 6–12 h).

Therefore, it can be concluded that the functionalization of SBA-15 with binary combinations of functional groups can be an ideal choice to enhance the adsorption-desorption of heavy metal ions. The use of such a bi-functional sorbent will allow complex treatment, removal and recycling of wastewater contaminated with different kinds of heavy metals and REEs.

## CRediT authorship contribution statement

**O. Dudarko:** Investigation, Conceptualization, Formal analysis, Methodology, Writing - original draft, preparation, Project administration, Funding acquisition. **N. Kobylinska:** Investigation, Formal analysis, Methodology, Writing - original draft, preparation. **B. Mishra:** Formal analysis, Investigation. **V.G. Kessler:** Resources, Writing - review & editing. **Bijay P. Tripathi:** Funding acquisition, Project administration, Writing - review & editing. **G.A. Seisenbaeva:** Validation, Supervision, Funding acquisition.

## Declaration of competing interest

The authors declare that they have no known competing financial interests or personal relationships that could have appeared to influence the work reported in this paper.

## Acknowledgments

Authors are grateful to the Ministry of Education and Education, Ukraine and Department of Science & Technology, Govt. Of India for financial support under the bilateral joint Ukraine-India R&D project (M-10/2020 and INT/UKR/P-27/2018), project "Multifunctional hybrid adsorbents for water purification". The work was also partially supported by the Swedish Research Council (Vetenskapsrådet) under the Swedish Research links Program, Dnr. 2018–2021. The authors are also indebted to the EU ERA-MIN 2 Program for support of the MetRecycle project (via Swedish Research Council Vinnova grant No. 2018–00739).

## Appendix A. Supplementary data

Supplementary data to this article can be found online at https://doi.org/10.1016/j.micromeso.2021.110919.

## References

[1] Y. Vystavna, Z. Frkova, H. Celle-Jeanton, D. Diadin, F. Huneaud, M. Steinmann, N. Crini, C. Loup, Sci. Total Environ. 637–638 (2018) 1358–1362, https://doi.org/10.1016/j.scitotenv.2018.05.095.
[2] F. Fu, Q. Wang, J. Environ. Manag. 92 (2011) 407–418, https://doi.org/10.1016/j.jenvman.2010.11.011.
[3] M.K. Uddin, Chem. Eng. J. 308 (2017) 438–462, https://doi.org/10.1016/j.cej.2016.09.029.
[4] R.T. Yang, Adsorbents: Fundamentals and Applications, Wiley-Interscience, New-Jersey, 2003.
[5] L.R. Radovic, C. Moreno-Castilla, J. Rivera-Utrilla, Chem. Phys. Carbon 27 (2001) 227–406, https://doi.org/10.1557/mrs2001.230.
[6] A.M. Liu, K. Hidajat, S. Kawi, Y. Zhao, Chem. Commun. (2000) 1145–1146, https://doi.org/10.1039/B002661L.

[7] A. Stein, B.J. Melde, R.C. Schroden, Adv. Mater. 12 (2000) 1403–1419, https://doi.org/10.1002/1521-4095(200010)12:19<1403::AID-ADMA1403>3.0.CO;2-X.
[8] D. Zhao, J. Feng, Q. Huo, N. Melosh, G.H. Fredrickson, B.F. Chmelka, G.D. Stucky, Science 279 (1998) 548–552, https://doi.org/10.1126/science.279.5350.548.
[9] Y. Ma, L. Qi, J. Ma, Y. Wu, O. Lin, H. Cheng, Colloid. Surface. 229 (2003) 1–8, https://doi.org/10.1016/j.colsurfa.2003.08.010.
[10] R. Roque-Malherbe, F. Marquez, Surf. Interface Anal. 37 (2005) 393–397, https://doi.org/10.1002/sia.2011.
[11] E. Da'na, A. Sayari, Chem. Eng. J. 166 (2011) 445–453, https://doi.org/10.1016/j.cej.2010.11.016.
[12] E. Da'na, Microporous Mesoporous Mater. 247 (2017) 145–157, https://doi.org/10.1016/j.micromeso.2017.03.050.
[13] D. Perez-Quintanilla, I. Del Hierro, M. Fajardo, I. Sierra, Microporous Mesoporous Mater. 89 (2006) 58–68, https://doi.org/10.1016/j.micromeso.2005.10.012.
[14] H.-M. Kao, T.-Y. Shen, J.-D. Wu, L.-P. Lee, Microporous Mesoporous Mater. 110 (2008) 461–471, https://doi.org/10.1016/j.micromeso.2007.06.035.
[15] X. Wang, K.S.K. Lin, J.C.C. Chan, S. Cheng, J. Phys. Chem. B 109 (2005) 1763–1769, https://doi.org/10.1021/jp045798d.
[16] Q. Yang, J. Yang, J. Liu, Y. Li, C. Li, Chem. Mater. 17 (2005) 3019–3024, https://doi.org/10.1021/cm050198s.
[17] Z. Gao, L. Wang, T. Qi, J. Chu, Y. Zhang, Colloids Surf., A 304 (2007) 77–81, https://doi.org/10.1016/j.colsurfa.2007.04.045.
[18] M.A. Markowitz, J. Klaehn, R.A. Hendel, S.B. Qadriq, S.L. Golledge, D.G. Castner, B.P. Gaber, J. Phys. Chem. B 104 (2000) 10820–10826, https://doi.org/10.1021/jp0008389.
[19] S. Ravi, Y.-R. Lee, K. Yu, J.-W. Ahn, W.-S. Ahn, Microporous Mesoporous Mater. 258 (2017) 62–71, https://doi.org/10.1016/j.micromeso.2017.09.006.
[20] I.V. Melnyk, V.P. Goncharyk, N.V. Stolyarchuk, L.I. Kozhara, A.S. Lunochkina, B. Alonso, Yu.L. Zub, J. Porous Mater. 19 (2012) 579–585, https://doi.org/10.1007/s10934-011-9508-3.
[21] L.S. Kostenko, N.G. Kobylinska, O. Khainakova, S. Garcia-Granda, Microchim. Acta. 186 (2019) 474, https://doi.org/10.1007/s00604-019-3520-8.
[22] O.A. Dudarko, V.P. Goncharik, V.Ya Semenii, Yu.L. Zub, Protect. Met. Phys. Chem. Surface 44 (2008) 193–197, https://doi.org/10.1134/S003317320802015X.
[23] N.A. Brunelli, Chem. Mater. 24 (2012) 2433–2442, https://doi.org/10.1021/cm300753z.
[24] E.L. Margelefsky, V. Dufaud, R.K. Zeidan, M.E. Davis, J. Am. Chem. Soc. 129 (2007) 13691–13697, https://doi.org/10.1021/ja074761e.
[25] L. Han, J. Ruan, Y. Li, O. Terasaki, S. Che, Chem. Mater. 19 (11) (2007) 2860–2867, https://doi.org/10.1021/cm0705845.
[26] J.M. Galloway, M. Kung, H.H. Kung, Surf. Sci. 648 (2016) 284–290, https://doi.org/10.1016/j.susc.2015.10.004.
[27] H. Suo, H. Duan, C. Chen, J.-C. Buffet, D. O'Hare, RSC Adv. 9 (2019) 3749–3754, https://doi.org/10.1039/C9RA00188C.
[28] R.K. Zeidan, M.E. Davis, J. Catal. 247 (2007) 379–382, https://doi.org/10.1016/j.jcat.2007.02.005.
[29] Y. Yang, A. Walton, R. Sheridan, K. Güth, R. Gauß, O. Gutfleisch, M. Buchert, B.-M. Steenari, T. Van Gerven, P.T. Jones, K. Binnemans, J. Sustain. Metall. 3 (2017) 122–149, https://doi.org/10.1007/s40831-016-0090-4.
[30] O.A. Dudarko, C. Gunathilake, N.P. Wickramaratne, V.V. Sliesarenko, Y.L. Zub, J. Górka, Sh Dai, M. Jaroniec, Colloids Surf., A 482 (2015) 1–8, https://doi.org/10.1016/j.colsurfa.2015.04.016.
[31] J.S. Brunauer, P.H. Emmet, E. Teller, J. Am. Chem. Soc. 60 (1938) 309–319, https://doi.org/10.1021/ja01269a023.
[32 ] E.P. Barrett, L.G. Joyner, P.P. Halenda, J. Am. Chem. Soc. 73 (1951) 373–380, https://doi.org/10.1021/ja01145a126.
[33] C. Nguyen, D.D. Do, Langmuir 15 (1999) 3608–3615, https://doi.org/10.1021/la981140d.
[34] V.M. Gun'ko, Appl. Surf. Sci. 307 (2014) 444–454, https://doi.org/10.1016/j.apsusc.2014.04.055.
[35] R. van Grieken, J.M. Escola, J. Moreno, R. Rodríguez, Chem. Eng. J. 155 (2009) 442–450, https://doi.org/10.1016/j.cej.2009.07.016.
[36] F. Rouquerol, J. Rouquerol, K.S.W. Sing, Adsorption by Powders and Porous Solids. Principles, Methodology and Applications, Academic Press, New York, 1999.
[37] G. Leofanti, M. Padovan, G. Tozzola, B. Venturelli, Catal. Today 41 (1998) 207–219, https://doi.org/10.1016/S0920–5861(98)00050–9.
[38] P. Van der Voort, P.I. Ravikovitch, K.P. De Jong, A.V. Neimark, A.H. Janssen, M. Benjelloun, E. Van Bavel, P. Cool, B.M. Weckhuysen, E.F. Vansant, Chem. Commun. 38 (2002) 1010–1011, https://doi.org/10.1039/B201424F.
[39] P. Van der Voort, P.I. Ravikovitch, K.P.D. Jong, M. Benjelloun, E.V. Bavel, A. H. Janssen, A.V. Neimark, B.M. Weckhuysen, E.F. Vansant, J. Phys. Chem. B 106 (2002) 5873–5877, https://doi.org/10.1021/jp025642i.
[40] Y. Wan, D. Zhao, Chem. Rev. 107 (2007) 2821–2860, https://doi.org/10.1021/cr068020s.
[41] A. Galarneau, H. Cambon, F. Di Renzo, F. Fajula, Langmuir 17 (2001) 8328–8335, https://doi.org/10.1021/la0105477.
[42] K.L. Jesenák, L. Kuchta, P. Hudec, V.S. Fagnor, J. Therm. Anal. Calorim. 55 (1999) 773–777, https://doi.org/10.1023/A:1010165313092.
[43] R.M. Silverstein, F.X. Webster, D.J. Kiemle, Spectrometric Identification of Organic Compounds, seventh ed., John Wiley &Sons, Inc., 2005.
[44] D. Lin-Vien, N.B. Colthup, W.G. Fateley, J.G. Grasselli (Eds.), The Handbook of Infrared and Raman Characteristic Frequencies of Organic Molecules, Acad. Press, London, 1991.
[45] V.N. Zaitsev, N.G. Kobylinskaya, L.S. Kostenko, V.I. Gerda, J. Anal. Chem. 63 (2008) 779–786, https://doi.org/10.1134/S1061934808080121.
[46] S.S. Dukhin, B.V. Derjaguin, in: E. Matijevic (Ed.), Electrokinetic Phenomena, Surface and Colloid Science, John Willey &Sons, NY, 1974.
[47] S. Barany, Adv. Colloid Interface Sci. 75 (1998) 45–78, https://doi.org/10.1016/S0001–8686(97)00043–2.
[48] S. Shen, P.S. Chow, S. Kim, K. Zhu, R.B.H. Tan, J. Colloid Interface Sci. 321 (2008) 365–372, https://doi.org/10.1016/j.jcis.2008.02.020.
[49] C.I. Lee, W.F. Yang, C.S. Chiou, J. Hazard Mater. 129 (2006) 58–63, https://doi.org/10.1016/j.jhazmat.2005.06.045.
[50] G. Anderegg, Critical Survey of Stability Constants of EDTA Complexes: Critical Evaluation of Equilibrium Constants in Solution: Stability Constants of Metal Complexes, Pergamon Press, 1977, https://doi.org/10.1016/C2013–0–02924–6.
[51] K. Ohshima, H. Watanabe, K. Haraguchi, Anal. Sci. 2 (1986) 131–135, https://doi.org/10.2116/analsci.2.131.
[52] T.P. Knepper, TrAC Trends Anal. Chem. (Reference Ed.) 22 (2003) 708–724, https://doi.org/10.1016/S0165-9936(03)01008-2.
[53] E. Polido Legaria, M. l Samouhos, V.G. Kessler, G.A. Seisenbaeva, Inorg. Chem. 56 (2017) 13938–13948, https://doi.org/10.1021/acs.inorgchem.7b02056.
[54 ] E. Polido Legaria, I. Saldan, P. Svedlindh, E. Wetterskog, K. Gunnarsson, V. G. Kessler, G.A. Seisenbaeva, Dalton Trans. 47 (2018) 1312–1320, https://doi.org/10.1039/C7DT04388K.
[55] K.R. Hall, L.C. Eagleton, A. Acrivos, T. Vermeulen, Ind. Eng. Chem. Fund. 5 (1966) 212–223, https://doi.org/10.1021/i160018a011.
[56] E. Repo, J.K. Warchol, T.A. Kurniawan, M.E.T. Sillanpaa, Chem. Eng. J. 161 (2010) 73–82, https://doi.org/10.1016/j.cej.2010.04.030.
[57] E. Da'na, A. Sayari, Desalination 285 (2012) 62–67, https://doi.org/10.1016/j.desal.2011.09.034.
[58 ] Z. Ezzeddine, I. Batonneau-Gener, Y. Pouilloux, H. Hamad, Z. Saad, V. Kazpard, Microporous Mesoporous Mater. 212 (2015) 125–136, https://doi.org/10.1016/j.micromeso.2015.03.013.
[59] J.P. Vareda, L. Durães, J. Sol. Gel Sci. Technol. 84 (2017) 400–408, https://doi.org/10.1007/s10971–017–4326–y.
[60] K.E. Engates, H.J. Shipley, Environ. Sci. Pollut. Res. 18 (2011) 386–395, https://doi.org/10.1007/s11356–010–0382–3.
[61] J. Thakkar, B. Wissler, N. Dudenas, X. Yin, M. Vailhe, J. Bricker, X. Zhang, Ind. Eng. Chem. Res. 58 (2019) 11121–11126, https://doi.org/10.1021/acs.iecr.9b02623.
[62] E.M. Abu Elgoud, Z.H. Ismail, M.I. Ahmad, Y.A. El-Nadi, S.M. Abdelwahab, H. F. Aly, Russ. J. Appl. Chem. 92 (2019) 1581–1592, https://doi.org/10.1134/S1070427219110156.
[63] Y. Pang, G. Zeng, L. Tang, Y. Zhang, Y. Liu, X. Lei, Z. Li, J. Zhang, G. Xie, Desalination 281 (2011) 278–284, https://doi.org/10.1016/j.desal.2011.08.001.
[64] X. Zheng, Y. Zhang, T. Bian, Y. Zhang, Z. Li, J. Pan, Chem. Eng. J. 381 (2020) 122669, https://doi.org/10.1016/j.cej.2019.122669.
[65] J. Gong, J. Feng, J. Liu, Z. Jiang, X. Chen, E. Mijowska, X. Wen, T. Tang, Chem. Eng. J. 248 (2014) 27–40, https://doi.org/10.1016/j.cej.2014.01.107.
[66] C. Zhang, J. Sui, J. Li, Y. Tang, W. Cai, Chem. Eng. J. 210 (2012) 45–52, https://doi.org/10.1016/j.cej.2012.08.062.
[67] S.-T. Yang, Y. Chang, H. Wang, G. Liu, S. Chen, Y. Wang, Y. Liu, A. Cao, J. Colloid Interface Sci. 351 (2010) 122–127, https://doi.org/10.1016/j.jcis.2010.07.042.
[68] Z. Yuna, Environ. Eng. Sci. 33 (2016) 443–454, https://doi.org/10.1089/ees.2015.0166.
[69] S. El Mourabit, M. Guillot, G. Toquer, J. Cambedouzou, F. Goettmann, A. Grandjean, RSC Adv. 2 (2012) 10916–10924, https://doi.org/10.1039/C2RA21569A.